

## DESIGN OF A PORTABLE ANTINEUTRINO DETECTOR FOR NUCLEAR REACTOR MONITORING

A. Ip<sup>1</sup>, A.B. McDonald<sup>1</sup>, G. Jonkmans<sup>2</sup> and B. Sur<sup>2</sup>

<sup>1</sup> Queen's University, Kingston, Ontario, Canada

<sup>2</sup> Atomic Energy of Canada Limited, Mississauga, Ontario, Canada

### Abstract

A design is proposed for a cubic metre scale antineutrino detector that can be deployed at ground level near a nuclear reactor. The lack of overburden necessitates good background rejection that is achieved using pulse shape discrimination and segmentation. A muon veto system and a large amount of neutron shielding are also used to discriminate against background. Antineutrinos are detected by inverse beta decay reactions in 75 liquid scintillator filled cells. A few simple modeling exercises are discussed, demonstrating the ability of the detector to detect both diversion of plutonium and fluctuations in reactor power by the change in antineutrino rate.

## 1. Introduction

### 1.1 Background and motivation

The International Atomic Energy Agency (IAEA) is a United Nations agency that aims to ensure peaceful development of nuclear energy. The goal of its safeguards regime is to verify the non-proliferation of nuclear weapons in particular by “timely detection” of a “significant quantity” of fissile material that may be used to produce nuclear weapons [1]. An antineutrino detector would allow unobtrusive, independent monitoring of the fuel composition of the reactor. Unexpected changes in the observed antineutrino flux could be related to the diversion of fissile material.

### 1.2 Design goal

The goal of this work is to produce a conceptual design for a portable antineutrino detector that may be used to monitor a nuclear reactor. It is assumed that the thermal power of the reactor is known and thus changes in the isotopic composition of the fuel may be determined by measuring the antineutrino rate [3]-[5]. Quantitatively, the detector should be able to detect a diversion of tens of kilograms of plutonium within a 90-day period. Large power fluctuations should be detected in less than a day.

Because of regulatory difficulties, reactor operators would likely be reluctant to place outside equipment within the reactor confinement. The aim is to contain the detector within a semi trailer or a shipping container, allowing it to be easily installed above ground near the reactor core without being overly intrusive.

## 2. Relevant physics

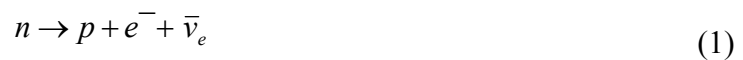
### 2.1 Production of antineutrinos

In a nuclear reactor, fission is induced in the uranium fuel. Incident neutrons cause  $^{235}\text{U}$  isotopes to split into two lighter, neutron-rich nuclei and free neutrons, the latter of which are able to induce further fissions. The fission products continue a  $\beta$ -decay chain, which produces antineutrinos. In addition to inducing further fission reactions, some of the neutrons are captured by  $^{238}\text{U}$  atoms, leading to the production of  $^{239}\text{Pu}$ , which is also a fissile isotope. Thus as  $^{235}\text{U}$  is consumed in the reactor, more  $^{239}\text{Pu}$  is produced (as is  $^{241}\text{Pu}$ ).

Table 1  
 Comparison of products of fissions by  $^{235}\text{U}$  and  $^{239}\text{Pu}$

	$^{235}\text{U}$	$^{239}\text{Pu}$
Release energy per fission	201.7 <i>MeV</i>	210.0 <i>MeV</i>
Mean energy of $\bar{\nu}_e$	1.46 <i>MeV</i>	1.32 <i>MeV</i>
$\bar{\nu}_e$ per fission $> 1.8 \text{ MeV}$	1.92	1.45

The fissions of  $^{239}\text{Pu}$  and  $^{235}\text{U}$  are similar, but the distributions of typical fission fragments produced are not identical and so the products of the  $\beta$ -decay chains have observable differences. The  $\beta^-$  decay process converts a neutron into a proton, emitting an electron and an antineutrino in the process.



The mean energy released per fission by  $^{239}\text{Pu}$  and  $^{235}\text{U}$  are slightly different, as is the average antineutrino flux, as shown in Table 1 [6] [7]. If the antineutrino rate is measured, then the isotopic composition of the reactor fuel may be determined if the thermal power is known or the antineutrino spectrum is also measured. Such measurements have been obtained using a prototype antineutrino detector at the San Onofre Nuclear Generating Station (SONGS) [3] [5]. That detector was placed in a “tendon” gallery approximately 25m away from the reactor core and 10m below ground.

### 2.2 Antineutrino detection

Inverse beta decay detection with organic liquid scintillators is the most common type of detection used for reactor antineutrinos [1] and was used in the SONGS1 detector [3], [8], [9]. Antineutrinos are detected through the inverse  $\beta$ -decay reaction between an antineutrino and a free proton in the medium.



This reaction has a threshold energy of  $\sim 1.8$  MeV and the (energy-dependent) cross section per target proton is on the order of  $10^{-43} \text{ cm}^2$ . The characteristic signal is the detection of a positron followed by the capture of a neutron shortly after. The neutron capture may occur on a proton, or the scintillator may be doped with a substance that has a high thermal neutron capture cross section, such as gadolinium. This helps to reduce the average capture time and Gd capture results in a large release of energy ( $\sim 8$  MeV) that can be easily detected.

### 2.3 Cosmic ray background

Cosmic rays provide the greatest challenge to an above ground detector because there is no overburden to reduce the background. An “antineutrino-like” signal may be generated by a fast neutron scatter from a proton (which resembles a positron signal) followed shortly by a neutron capture event. It is possible to distinguish between these events because proton recoils and positron events have differences in the time profiles of the pulses created, as will be discussed later.

Muons that travel through a detector and its surrounding material may produce a background signal themselves as they pass through the detector or through secondary interactions. This includes the production of fast neutrons through muon spallation and muon induced cosmogenic radioactivity [10]. The main concern for this detector is the production of fast neutrons since they may produce false antineutrino signals.

The flux of muons at ground level is increased by 5 to 10 times compared to the level at SONGS1 (where there was  $\sim 25$  meters of water equivalent overburden) [8]. There are many measurements of sea level muon flux in the literature [11], with the reported fluences not always in agreement [12]. A commonly accepted value for sea level vertical flux intensity for muons above 1 GeV is  $70 \text{ m}^{-2}\text{s}^{-1} \text{ sr}^{-1}$  [13]. The angular distribution roughly follows a  $\cos^2 \theta$  distribution relative to the vertical [14], giving an intensity of  $\sim 110 \text{ m}^{-2}\text{s}^{-1}$  for muons above 1 GeV. At lower energies, the flux can be affected by geomagnetic effects and solar influences, creating more variation in measured muon flux [14][15] [16].

Cosmic neutrons are increased by about 10 times at the surface compared to the SONGS1 site, with the thermal neutron flux increasing by 2 or 3 orders of magnitude [17]. Measurements of sea level neutron flux range span a range from  $63 \text{ m}^{-2}\text{s}^{-1}$  to  $200 \text{ m}^{-2}\text{s}^{-1}$  [14] [15][18] [19]. Differences in measured neutron fluences can be explained by variations in local atmospheric pressure and temperature, as well as changes in solar activity.

### 3. Detector design

#### 3.1 Overview

The detector design presented here was influenced strongly by the SONGS1 design [8]. The main considerations were determining how to deal with the increased background and how to make use of different geometry. Whereas SONGS1 was located in an underground tendon gallery inside the reactor confinement, this detector is to be placed above ground. It was decided that the detector should be housed within a shipping container since they are readily available, and can be easily transported and placed on the reactor grounds. A standard 20ft shipping container has internal dimensions  $2.34W \times 2.4H \times 5.9L$  m<sup>3</sup>.

The active volume consists of liquid scintillator filled cells. Each cell is read out by a PMT and every pulse that passes a simple hardware discrimination is read out to a digital data acquisition system. Further cuts are applied in software in order to distinguish antineutrino events. The main volume is surrounded by an active muon veto system and a passive polyethylene shield. A rendering of the design is shown in Figure 1.

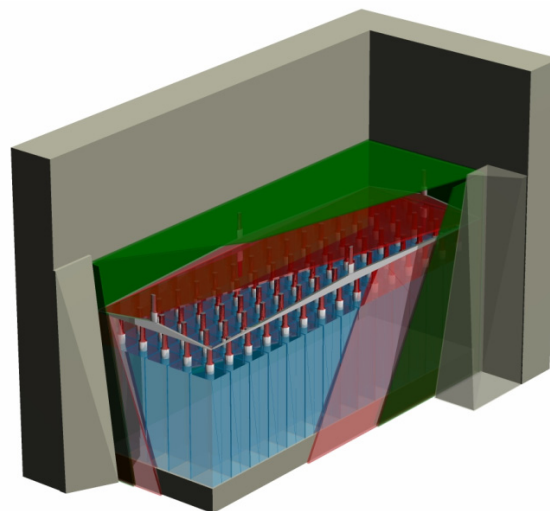


Figure 1 Cutaway rendering of detector design. Active volume cells are blue, muon veto system is red, borated polyethylene is green and pure polyethylene is grey.

In order to deal with the increased amount of neutron background present at the surface, this design utilizes pulse shape discrimination to reject fast neutron scatterings that resemble positron events. A muon veto system is used to discriminate against muon-induced events; however, the veto system is placed inside the passive shielding in order to match it to the size of the central scintillator volume. This is necessary to reduce the dead time of the detector by reducing the number of muons triggering the veto system. Simply placing the SONGS1 design (which had the muon veto around the passive shielding) at the surface could result in a dead time as high as 50% [17], making it essentially unusable.

## 3.2 Active volume

### 3.2.1 Scintillator

There were a number of concerns to be addressed when choosing a liquid scintillator. First, it was desired that the scintillator have pulse shape discrimination capability in order to separate positron events from the fast neutron scattering background. The safety aspects of the scintillator are also important, particularly since the detector will be placed on the nuclear plant grounds. A liquid scintillator with a high flashpoint and low toxicity is preferable.

For this detector, a linear alkylbenzene (LAB) scintillator was chosen. LAB is attractive because it has a high flashpoint (130°C) and low toxicity [20]. It is also relatively cheap because of its common use in other products such as detergents; LAB scintillator costs approximately \$1600 per tonne [21]. The density is 0.86g/cm<sup>3</sup> [20] and the typical molecule contains 18 carbon atoms and 30 hydrogen atoms. This gives a hydrogen density of  $6.3 \times 10^{22}$  H/cm<sup>3</sup>.

The pulse shape discrimination ability of LAB has not been fully investigated, but initial tests suggest that n/γ discrimination is possible [20]. The effectiveness of PSD is affected by the length of the scintillator cell, but it still works with about 90% efficiency at distances of approximately 50cm [17], [23]. To improve the thermal neutron capture abilities, the scintillator will be doped with 0.1%wt gadolinium. The thermal neutron absorption cross-section for <sup>157</sup>Gd is 255000 barns [24]; the capture cross-section for natural abundance gadolinium is 49000 barns [25]. The addition of gadolinium serves to reduce the mean capture time of thermal neutrons to ~ 27μs from > 200μs. Approximately 89% of the captures occur on Gd, producing a large ~8MeV signal [25]. The remainder occur on protons, producing a 2.2MeV signal [8].

It has been shown in the literature that a 0.2%wt Gd doped LAB scintillator has very good chemical stability for a period of at least 6 months [25], and in fact remains stable well beyond that time [26]. Gadolinium doping techniques for LAB are being developed at Brookhaven National Laboratory [25], [26].

### 3.2.2 Cells

The scintillator will be contained within stainless steel cells coated with Teflon. Each cell measures 25 × 25 × 50 cm<sup>3</sup> with 5mm thick walls. The volume of scintillator in each cell is approximately 28.2L. A 9-inch hemispherical PMT detects the scintillation light through an acrylic coupling cylinder submerged into the cell at one end. The smaller cells help accomplish two goals. First, the size makes it possible to use pulse shape discrimination to reject fast neutron background. Secondly, the increased segmentation allows better rejection of random background producing a delayed coincidence event.

The cells will be oriented vertically (longest dimension in vertical direction) with the PMT located on top. To remain within the confines of a shipping container, the active volume is 5 cells wide and 15 cells long (or 1.25m wide × 3.75m long). This leaves over half a meter for shielding and other components on each side while giving a total scintillator volume of ~ 2.1m<sup>3</sup>.

### 3.3 Muon veto

The muon veto system consists of the same design used in the SONGS1 detector [8]. Instead of surrounding all of the passive shielding, the veto system only surrounds the central active volume. Plastic scintillator paddles 2cm thick cover the cell array on five sides, with the side sections extending to cover the area beneath the detector. A veto system on the bottom is not necessary because the muon flux is downward and goes to zero at  $90^\circ$  to the vertical [14]. The top section covers an area of  $4.69\text{m}^2$  and the sides cover  $10\text{m}^2$ . Due to the  $\cos^2 \theta$  distribution of muon flux, the number of counts in a vertically oriented side panel will be half that of a horizontal panel of the same area. Thus the effective area of the muon veto can be taken as  $9.69\text{m}^2$ .

Muons continuously lose energy by ionization as they travel through matter at an approximate rate of  $2\text{MeV}/(\text{g cm}^{-2})$  [27]. Since plastic scintillators typically have a density of  $\sim 1\text{g}/\text{cm}^3$  [24], muons passing through the veto will deposit at least  $4\text{MeV}$  of energy which can easily be detected to trigger a veto. SONGS1 used a veto time for the antineutrino data of  $100\mu\text{s}$  following a muon event. They calculated that such a cut would exclude 99.3% of events correlated with a muon that was detected in the veto system.

### 3.4 Passive shielding

The SONGS1 design used approximately 0.5m of shielding consisting of water and polyethylene; simulations suggested that  $10\text{MeV}$  neutron flux was reduced by a factor of 25 and  $2\text{MeV}$   $\gamma$ -rays by a factor of 10 [8]. Attenuation data for pure polyethylene shielding provided by Shieldwerx [28] indicated that 99% of  $20\text{MeV}$  neutrons would be attenuated after 45cm. For cost considerations, water is a cheap alternative to polyethylene as a fast neutron moderator. It may also reduce transportation loads if the water is obtained on site to fill shielding cells. However, neither pure polyethylene nor water absorbs many of the thermal neutrons. The addition of boron can be used to capture slow neutrons in the shielding since  $^{10}\text{B}$  has a high thermal neutron cross section of 3840 barns [24]. The best method would be to have a layer inside the neutron moderating material to absorb the thermalized neutrons.

For this design, 2.5cm of borated polyethylene immediately surrounds the muon veto system. Underneath the cell array (and within the side panels of the muon veto), a 25cm layer of polyethylene is used for shielding. On the sides, 47.5cm of pure polyethylene moderates the neutron flux outside the borated layer. Above the detector, approximately a meter of polyethylene shielding is employed. This makes use of the space available in a shipping container (which is 2.4m high) and compensates for a stronger neutron intensity in the vertical direction. Similar to muons, the cosmic neutron flux has a zenith angle dependence of  $\cos^{2.7} \theta$  [29]. Another consequence of this distribution is that cosmic neutrons will rarely pass through the side shielding at  $90^\circ$ ; thus the path through the shielding is typically longer than the shielding thickness. This shielding will essentially eliminate slow neutrons and 1m of polyethylene should reduce  $20\text{MeV}$  neutrons through the top of the detector by up to 4 orders of magnitude. More specific calculations of the neutron flux through the shielding will require the use of neutron transport simulation codes, which is beyond the scope of this project.

#### 4. Expected performance

The number of antineutrino events that occur in the detector depends on many factors, including the fission rates of each isotope and the geometry of the system. The total number of antineutrino interactions,  $N_{\bar{\nu}}$ , in a time interval,  $T$ , can be found by:

$$N_{\bar{\nu}} = \left(\frac{TN_p}{4\pi D^2}\right) \sum_i f_i \int dE_{\bar{\nu}} \sigma(E_{\bar{\nu}}) \phi_i(E_{\bar{\nu}}) \varepsilon(E_{\bar{\nu}}) \quad (3)$$

where  $N_p$  is the number of target protons in the detector,  $D$  is the distance from the detector to the reactor core,  $f_i$  is the number of fissions per second from the  $i$ th isotope,  $\sigma$  is the energy dependent inverse  $\beta$ -decay interaction cross section,  $\phi_i$  is the antineutrino number density per  $MeV$  per fission of the  $i$ th isotope and  $\varepsilon$  is a detection efficiency factor. The index  $i$  runs over the dominant fissioning isotopes in the reactor, typically  $^{235}\text{U}$ ,  $^{238}\text{U}$ ,  $^{239}\text{Pu}$  and  $^{241}\text{Pu}$  [8].

The inverse  $\beta$ -decay cross section can be adequately described by:

$$\sigma(E_{\bar{\nu}}) = \frac{0.0952}{1MeV^2} (E_{\bar{\nu}} - \Delta) \left[ E_{\bar{\nu}}^2 - E_{\bar{\nu}}\Delta + \Delta^2 - m_e^2 \right]^{\frac{1}{2}} \times 10^{-42} cm^2 \quad (4)$$

where  $\Delta$  is the difference between the neutron and proton masses ( $\sim 1.294\text{Mev}/c^2$ ) and  $m_e$  is the positron mass [30]. The spectrum of element  $i$ ,  $\phi_i(E_{\bar{\nu}})$ , can be described by a fit of the form:

$$\phi_i(E_{\bar{\nu}}) = \exp \left[ \sum_{k=1}^6 a_{ki} E_{\bar{\nu}}^{k-1} \right] \quad (5)$$

with the coefficients  $a_{ki}$  for  $^{235}\text{U}$ ,  $^{239}\text{Pu}$  and  $^{241}\text{Pu}$  provided by Huber and Schwetz [31].

To create a simple model of the expected antineutrino rates, Equations 3, 4, and 5 were applied for the two main fissioning isotopes,  $^{235}\text{U}$  and  $^{239}\text{Pu}$ . The isotope ratio and the thermal power of the reactor could be adjusted in order to create the expected antineutrino spectrum and calculate the total number of counts per day (for a perfectly efficient detector). By setting the ratio of  $^{235}\text{U}$  to  $^{239}\text{Pu}$  to 9:1 and setting the thermal power to 3.4GWth (as at the San Onofre plant), approximately 3600 counts per day were expected for a detector similar to SONGS1. The predicted amount for SONGS1 was  $3800 \pm 440$  [8], so the simple model used for this project seems to produce a reasonably accurate estimate.

For the same reactor model, there are about 9980 expected interactions per day in the designed detector due to the larger active volume. For a 2100 MWth CANDU reactor, with 50% of the power coming from each of  $^{235}\text{U}$  and  $^{239}\text{Pu}$ , the number of expected interactions is 5084.

#### 4.1 Positron event

The positron event, also called the “prompt” event, occurs essentially instantaneously after the inverse  $\beta$ -decay interaction as the positron quickly thermalizes and annihilates with an electron. The energy deposited is called the prompt energy,  $E_{prompt}$ . The antineutrino energy can be related to the prompt energy by:

$$E_{\bar{\nu}} = E_{prompt} + 1.8MeV - 2m_e \quad (6)$$

Unfortunately, interactions near the edge of the detector may result in the escape of annihilation  $\gamma$ -rays. Using Monte Carlo simulations, it is possible to account for these losses as well as obtain an estimate of the detection efficiency of the prompt energy [8].

As previously mentioned, it is possible for a proton recoil following a fast neutron scatter to mimic a positron event in some systems. These events are rejected using pulse shape discrimination (PSD) in this design. PSD is possible because the shape of each scintillation pulse is composed of both a fast and a slow component. Each component may be adequately modeled as an exponential decay, with the decay times being a few nanoseconds compared to hundreds of nanoseconds for the fast and slow components respectively. The majority of the light yield occurs in the fast component, but the fraction of light in the slow component typically depends on the exciting particle [24]. This is shown in Figure 2. Pulse shape discrimination can be applied using analogue methods (in hardware) or, more recently, using digital methods (in software) [22], [32]. Digital PSD will be used for this detector, as it generally meets or exceeds the capabilities of analogue methods [32]. The effectiveness of PSD is estimated to be 90% for this design.

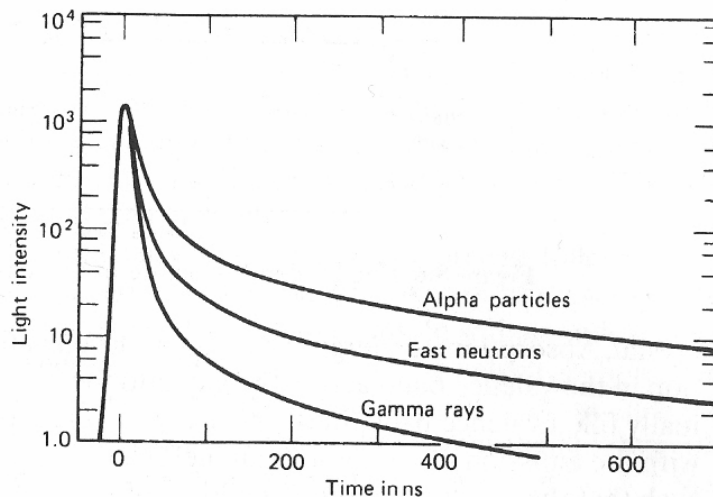


Figure 2 Example of time dependence of scintillation pulses by different sources [24]

In addition to using pulse shape discrimination, positron events are distinguished by applying energy cuts to any pulses that pass the PSD requirement. The specific energy thresholds would be chosen to optimize the signal to background ratio and to maintain long term stability of the threshold energy. For instance, SONGS1 used a lower positron energy threshold of  $2.39\text{MeV}$  to match the calibration peak from  $^{208}\text{Tl}$   $\gamma$ -rays [8], and such a threshold is reasonable for this detector as well. This maintains a stable threshold value and cuts out significant low energy background, including the  $2.2\text{MeV}$   $\gamma$ -ray peak expected from neutron capture on hydrogen in the scintillator or shielding. Since the expected prompt energy spectrum begins at around  $1\text{MeV}$  (as can be seen from Equation 6), approximately 25% of all antineutrino related positron events are cut. Since there are very few prompt events with energy greater than  $8\text{MeV}$ , a high threshold is set. The SONGS1 detector implemented a high threshold of  $9\text{MeV}$  and attained a positron detection efficiency of  $55 \pm 5\%$ , or approximately 75% of the events not eliminated by energy cuts [8]. It is reasonable to expect this detector to at least match this efficiency.

## 4.2 Neutron event

In addition to the positron, an inverse  $\beta$ -decay event produces a neutron with a small amount of kinetic energy, in the range of 1 to 50 keV [2], [8]. The “delayed” event is characterized by the capture of the thermalized neutron on gadolinium, producing an  $8\text{MeV}$   $\gamma$ -ray shower [25]. As stated before, only 89% of neutron captures occur on Gd, the rest occur on protons and do not produce the characteristic  $8\text{MeV}$  signal.

The  $\gamma$ -rays produced by the Gd capture typically have energies of about  $2\text{MeV}$  [33]. As with the prompt event, some  $\gamma$ -rays may escape the active volume without depositing the full energy. To account for this loss, a lower threshold energy can be set; SONGS1 used a lower threshold of  $3.5\text{MeV}$  to optimize neutron detection efficiency while minimizing statistical uncertainty [8]. A high threshold around  $10\text{MeV}$  is chosen to account for the highest energy released due to the thermal neutron capture and the energy resolution of the cells. The SONGS1 detection efficiency for neutrons was  $40 \pm 4\%$ ; this is likely due to the lower threshold cutting a large number of neutron events. In this detector, since the segmentation and pulse shape discrimination help to reduce the random background, it may be possible to use a lower threshold (at around  $2.5\text{MeV}$ ) while maintaining a similar signal to noise ratio as SONGS1. It is therefore reasonable to expect a neutron detection efficiency of around 50%.

In addition to neutrons “lost” to capture on protons, inverse  $\beta$ -decay events that occur near the edge of the active volume may result in neutrons that escape from the scintillator before thermalization and capture. The fiducial volume is estimated to be 74% of the total. Once again, a better estimate of this effect can be obtained using neutron transport simulations.

## 4.3 Background rejection

As discussed in the previous section, the polyethylene shield (and borated poly layer) reduces the flux of neutrons  $\leq 20\text{MeV}$  by a substantial amount. Higher energy flux will be reduced by

the shielding and it is likely that some very high energy neutrons will pass through the detector without interacting due to the low cross section. Pulse shape discrimination can be expected to drop positron-mimicking events by a factor of 10 [17]. The discussed energy cuts will also reduce this background; in fact,  $1\text{MeV}$  neutrons would not deposit enough energy to pass the prompt energy threshold and neutrons in the correct energy range would have smaller cross sections.

Since the muon veto is inside the polyethylene shielding, one concern is that muons passing through the passive shield will induce a large number of fast neutrons. However, muon induced fast neutron production is of primary concern in high atomic number materials such as lead [35]. In polyethylene, the production of neutrons is  $2.382 \times 10^{-4} n/\mu(\text{g}/\text{cm}^2)$ , which is quite low [36]. In addition, the neutrons produced are attenuated by the polyethylene, so the contribution of neutrons induced in the passive shielding can be considered negligible.

The muon veto of the SONGS1 system was  $91 \pm 0.2\%$  efficient. Considering the 90% effectiveness of PSD, muon induced neutrons inside the active volume are reduced by over 100 times. Adding energy cuts further reduces this component. The deadtime induced depends on the exact flux of muons at the surface. A lower estimate of  $160\text{m}^{-2}\text{s}^{-1}$  yields a dead time of approximately 15.5%. A large muon flux estimate of  $300\text{m}^{-2}\text{s}^{-1}$  would increase the deadtime to about 29%.

#### 4.4 Antineutrino event selection

To determine which event pairs are caused by antineutrinos, further processing is done in software. From all the events recorded and identified as potential prompt or delayed events, candidate pairs of events are created. Two more cuts are then applied: a temporal cut and a spatial cut.

The temporal cut requires the positron annihilation and neutron capture to occur in close time coincidence. Whereas the positron event occurs almost instantaneously after the inverse  $\beta$  interaction, the time to capture on Gd follows an exponential decay distribution with a time constant of about  $27\mu\text{s}$  following thermalization. For this detector, a time cut will be imposed for 5 to  $100\mu\text{s}$  to allow enough thermalization time [34] and maintain about 80% of events.

The spatial cut eliminates many uncorrelated events that are caused by two random single events mimicking an antineutrino. The higher degree of segmentation should help reduce the rate of random coincidence events. This enables lower thresholds to be employed to improve the detector efficiency while maintaining a usable signal-to-noise ratio.

### 5. Discussion

#### 5.1 Efficiency and scenario models

An estimate of the overall efficiency of the detector as described is shown in Table 2. The efficiency is approximately 13%, similar to the SONGS1 efficiency of  $10.7 \pm 1.5\%$  [8]. The

largest drop in efficiency was due to the longer induced dead time, as expected. This was primarily compensated for by introducing pulse shape discrimination. The neutron efficiency is expected to be improved with a lower energy threshold imposed. The positron efficiency was assumed to be the same as the SONGS1 detector. Simulations would be required to determine a more accurate estimate of the detector efficiency. Due to the energy cuts, positron efficiency has an upper limit of about 75% while neutron efficiency is limited to < 89% due to capture on protons as well as energy cuts.

Table 2  
 Detection Efficiency

Quantity	Efficiency
Positron	$55 \pm 10\%$
Neutron	$50 \pm 10\%$
Time Cut	$80 \pm 3\%$
Fiducial	$74 \pm 5\%$
Live time	$\sim 78 \pm 8\%$
Total	$13 \pm 4\%$

Using this efficiency value and the reactor spectrum model described earlier, it is possible to make a few simple calculations of the detector performance. It is assumed that the signal-to-noise ratio is 4:1, approximately the ratio obtained at SONGS1 [8].

The first model is for a CANDU style reactor that is operating at 2.1GWth. Since CANDU reactors are refuelled online, plutonium diversion is a larger concern. At about mid burnup, the power contributed from each of  $^{235}\text{U}$  and  $^{239}\text{Pu}$  is approximately equal. Thus, based on the average nuclide densities, there is  $\sim 320\text{kg } ^{235}\text{U}$  and  $\sim 200\text{kg } ^{239}\text{Pu}$  [38]. In our model, the initial condition consisted of  $324\text{kg } ^{235}\text{U}$  and  $198\text{kg } ^{239}\text{Pu}$ . At these conditions, 672 counts are expected per day. A 30kg diversion of plutonium results in a small change in expected counts to 638, a difference of 34 counts. Using Poisson statistics and the assumed 4:1 signal-to-noise ratio,  $\sigma=29$ , so the diversion can be detected after one day to a  $1\sigma$  level. For a  $3\sigma$  level, about 7 days of counting are required.

A more difficult to detect case is if plutonium is diverted while uranium is added to the core, thus maintaining the same power output. A scenario was modeled in which 20kg of  $^{239}\text{Pu}$  was diverted while 28kg of  $^{235}\text{U}$  was added in the CANDU reactor. In this case, the daily count rate increased by about 16 events per day; thus, it would take 4 days of counting for a  $1\sigma$  difference to be observed. A  $3\sigma$  change would be observed after 33 days, assuming reactor conditions remain constant. A third scenario tested was a power change in a 3.4GWth pressurized water reactor (PWR). Since such reactors must be refuelled offline, it is more important to be able to detect variations in power output. The modeled reactor had a mass ratio of 9 to 1 for  $^{235}\text{U}$  to  $^{239}\text{Pu}$ . If the power was suddenly dropped to 80% of capacity (2.72GWth), the change would be detected to  $1\sigma$  and  $3\sigma$  levels in 1 and 8 hours respectively.

Based on the results of these calculations, this detector would be able to meet the stated goal of detecting the diversion of tens of kilograms of plutonium. It would also quickly be able to identify large power fluctuations. Note that due to the simplifications of the model, the time scales may be slightly optimistic for anomaly detection. For instance, only two core isotopes were considered whereas there are other contributions that would affect the count rates.

## 6. Conclusion

A conceptual design has been described here with the goal of detecting reactor power fluctuations and diversion of nuclear material. The SONGS1 detector was used as a starting point for the design, with adjustments made to account for the increased background rates at the surface. Pulse shape discrimination and increased shielding were used to significantly reduce the fast neutron background. The muon veto system was placed inside the neutron shielding in order to keep veto induced dead time to a minimum. The reactor is monitored by the antineutrino event rate. In principle, it is possible to use the antineutrino energy spectrum to gain a fuller understanding of the fissile inventory, but it is more difficult to implement. Such measurements would require over 3000 counts per day [39]. Simple modelling was presented to predict the behaviour of the detector. Monte Carlo simulations are recommended to better characterize the expected performance.

The design presented here demonstrates that it is feasible to use an antineutrino detector at the surface to monitor a nuclear reactor. Such a detector may be deployed easily at any reactor site without requiring the use of an underground area within reactor confinement. Additionally, the design is scalable to meet specific needs at various deployment locations and budget constraints. The monitoring ability afforded by the proposed detector could be a useful addition to the IAEA safeguards regime.

## 7. References

- [1] A. Bernstein, G. Baldwin, B. Boyer, M. Goodman, J. Learned, J. Lund, R. Svoboda, and D. Reyna, Tech. Rep., IAEA (2008), in draft form as part of IAEA preparatory paper for Focused Workshop on Antineutrino Detection for Safeguards Applications.
- [2] F. Boehm, J. Busenitz, B. Cook, G. Gratta, H. Henrikson, J. Kornis, D. Lawrence, K. B. Lee, K. McKinny, L. Miller, et al., Phys. Rev. D 64, 112001 (2001)
- [3] A. Bernstein, N. Bowden, A. Misner, and T. Palmer, Journal of Applied Physics 103 (2008)
- [4] M. Cribier (2007), XXII International Conference On Neutrino Physics And Astrophysics
- [5] N. Bowden, A. Bernstein, S. Dazeley, R. Svoboda, A. Misner, and T. Palmer, Observation of the isotopic evolution of PWR fuel using an antineutrino detector (2008), arXiv:0808.0638v1 [nucl-ex].
- [6] M. Cribier, Earth, Moon, and Planets 99 (2006)

- [7] S. Cormon, F. S, L. Giot, B. Guillon, J. Martino, D. Lhuillier, A. Letourneau, T. Mueller, M. Cribier, and T. Lasserre, Effort on the simulation of the antineutrino spectrum from reactor, AAP Workshop 2007 Slides (2007)
- [8] N. Bowden, A. Bernstein, J. Brennan, M. Cunningham, J. Estrada, C. Greaves, C. Hagmann, J. Lund, T. Weinbeck, and C. Winant, Nucl.Instrum.Meth. A572, 985 (2007)
- [9] J. Lund, An alternative design based on inverse beta detection, Presentation Slides (2007), from Applied Antineutrino Physics Workshop.
- [10] D.-M. Mei and A. Hime, Physical Review D (Particles and Fields) 73, 053004 (page 18) (2006)
- [11] T. Hebbeker and C. Timmermans, Astroparticle Physics 18, 107 (2002)
- [12] E. Bugaev, A. Misaki, V. Naumov, T. Sinegovskaya, S. Sinegovsky, and N. Takahashi, Physical Review D 58 (1998)
- [13] T. Gaisser and T. Stanev, Physics Letters B 667, 254 (2008)
- [14] L. Bogdanova, M. Gavrilov, V. Kornoukhov, and A. Starostin, Phys. Atom. Nucl. 69, 1293 (2006).
- [15] R. Wordel, D. Mouchel, T. Altzitzoglou, G. Heusser, B. Quintana Arnes, and P. Meynendonckx, Nucl.Instrum.Meth. A369, 557 (1996)
- [16] H. Malm, M. Watt, I. Bostock, J. Campbell, P. Jagam, and J. Simpson, Nuclear Instruments and Methods in Physics Research 223, 420 (1984)
- [17] D. Reyna and N. Bowden, Private communication (Jan 20, 2009)
- [18] T. Nakamura, T. Nunomiya, S. ABE, K. Terunuma, and H. Suzuki, Journal of Nuclear Science and Technology 42, 843 (2005)
- [19] R. Wordel, D. Mouchel, E. Steinbauer, and R. Oyrer, Appl. Radiat. Isot. 47, 1061 (1996)
- [20] Petresa Canada, Linear alkylbenzene MSDS, Datasheet (2008)
- [21] M. Chen, Private communication (2009)
- [22] R. Winyard and G. McBeth, Nucl.Instrum.Meth. 98 (1972)
- [23] G. Zacek, F. Feilitzsch, R. Mossbauer, L. Oberauer, V. Zacek, F. Boehm, P. Fisher, J. Gimlett, A. Hahn, H. Henrikson, et al., Phys. Rev. D 34 (1986)
- [24] G. Knoll, Radiation Detection and Measurement (John Wiley & Sons, Inc., 2000), 3<sup>rd</sup> ed
- [25] M. Yeh, A. Garnov, and R. Hahn, Nuclear Instruments and Methods in Physics Research A 578, 329 (2007)
- [26] R. Hahn, Private communication (2009).

- [27] T. Gaisser, *Cosmic Rays and Particle Physics* (Cambridge University Press, 1990)
- [28] Shieldwerx, SWX-201 (5% Boron-Poly) and SWX-213 (Pure Poly) Properties and Radiation Thickness Calculator (2008)
- [29] N. Mascarenhas, J. Brennan, K. Krenz, P. Marleau, and S. Mrowka, in 2007 IEEE Nuclear Science Symposium Conference Record (2007)
- [30] P. Vogel and J. Beacom, *Physical Review D* 60 (1999)
- [31] P. Huber and T. Schwetz, *Phys. Rev. D* 70, 053011 (2004)
- [32] P. Soderstrom, J. Nyberg, and R. Wolters, *Nucl. Instrum. Meth. A*594, 79 (2008)
- [33] E. Toubetzko, *Physical Review* 122, 212 (1961)
- [34] W. Nellis, *American Journal of Physics* 45 (1977)
- [35] V. Chazal, F. Boehm, B. Cook, H. Henrikson, G. Jonkmans, A. Paic, N. Mascarenhas, P. Vogel, and J.L. Vuilleumier, *Nucl. Instrum. Meth. A*490, 334 (2002)
- [36] H. Wulundari, J. Jochum, W. Rau, and F. von Feilitzsch, arXiv:hep-ex/0401032v1 (2004)
- [37] S. Marrone, D. Cano-Ott, N. Colonna, C. Domingo, F. Gramegna, E. Gonzalez, F. Gunsing, M. Heil, F. Kappeler, P. Mastinu, et al., *Nucl. Instrum. and Meth. A*490, 299 (2002)
- [38] J. Whitlock, Private communication (2009)
- [39] IAEA, Final report: Focused workshop on antineutrino detection of safeguards applications (2008)